The Astronomical Journal, 153:137 (11pp), 2017 March https://doi.org/10.3847/1538-3881/aa5d10

Is There a Circumbinary Planet around NSVS 14256825?

Ilham Nasiroglu[1], Krzysztof Goździewski[2], Aga Słowikowska[3], Krzysztof Krzeszowski[3], Michał Żejmo[3], Staszek Zola[4], Huseyin Er[1], Waldemar Ogłoza[5], Marek Dróżdż[5], Dorota Koziel-Wierzbowska[4], Bartlomiej Debski[4], and Nazli Karaman[6]
[1] Departments of Astronomy and Astrophysics, Ataturk University Yakutiye, 25240, Erzurum, Turkey; aga@astro.ia.uz.zgora.pl
[2] Centre for Astronomy, Faculty of Physics, Astronomy and Applied Informatics, N. Copernicus University, Grudziadzka 5, 87-100 Toruń, Poland
[3] Janusz Gil Institute of Astronomy, University of Zielona Góra, Prof. Szafrana 2, 65-516 Zielona Góra, Poland
[4] Astronomical Observatory, Jagiellonian University, Orla 171, 30-244 Kraków, Poland
[5] Mt. Suhora Observatory, Pedegogical University, Podchorazych 2, 30-084 Kraków, Poland
[6] Physics Department, Adiyaman University, Merkez, 02040, Adiyaman, Turkey
Received 2016 December 7; revised 2017 January 7; accepted 2017 January 18; published 2017 March 2

Abstract

The cyclic behavior of (O–C) residuals of eclipse timings in the sdB+M eclipsing binary NSVS 14256825 was previously attributed to one or two Jovian-type circumbinary planets. We report 83 new eclipse timings that not only fill in the gaps in those already published but also extend the time span of the (O–C) diagram by three years. Based on the archival and our new data spanning over more than 17 years, we re-examined the up-to-date system (O–C). The data revealed a systematic, quasi-sinusoidal variation deviating from an older linear ephemeris by about 100 s. It also exhibits a maximum in the (O–C) near JD 2,456,400 that was previously unknown. We consider two most credible explanations of the (O–C) variability: the light propagation time due to the presence of an invisible companion in a distant circumbinary orbit, and magnetic cycles reshaping one of the binary components, known as the Applegate or Lanza–Rodonó effect. We found that the latter mechanism is unlikely due to the insufficient energy budget of the M-dwarf secondary. In the framework of the third-body hypothesis, we obtained meaningful constraints on the Keplerian parameters of a putative companion and its mass. Our best-fitting model indicates that the observed quasi-periodic (O–C) variability can be explained by the presence of a brown dwarf with the minimal mass of 15 Jupiter masses rather than a planet, orbiting the binary in a moderately elliptical orbit ($e \simeq 0.175$) with a period of $\sim$10 years. Our analysis rules out the two-planet model proposed earlier.

Key words: binaries: close – binaries: eclipsing – planets and satellites: detection – stars: individual (NSVS 14256825) – subdwarfs

Supporting material: machine-readable tables, tar.gz file

1. Introduction

The number of discovered exoplanets around binary systems increases rapidly. These discoveries have sparked a rising interest in this subject among researchers, and consequently, they drive the development of new detection techniques. Studies of circumbinary planets (CBPs) have taken us much closer toward answering the fundamental questions of how such planets form and evolve. The properties of CBPs are likely different than these orbiting isolated stars (Lee et al. 2009).

The most remarkable discovery made with the transit method with the *Kepler* satellite is the discovery of a CBP transiting across both stars of the close binary system Kepler-16 (AB; Doyle et al. 2011). The transits in this system leave no doubt about the existence of planets in the so-called "P-type" orbits, i.e., circumbinary orbits. So far, the longest-period transiting CBP is Kepler-1647 with the orbital period of $\sim$1100 days (Kostov et al. 2016b).

Even before the *Kepler* discoveries, timing observations have provided evidence of planets orbiting binary systems. Hints for such companions were reported by Deeg et al. (2008) and Lee et al. (2009) for the eclipsing binaries CM Dra and HW Vir, respectively. The presence of these objects is indicated through the Light Travel Time (LTT) effect indicated by the variations in the timings of eclipse minima w.r.t. the linear ephemeris (O–C). Quasi-periodic variations of the (O–C) can result from the gravitational tug due to distant planets (companions), which leads to swinging of the eclipsing binary, and causing the eclipses to appear slightly earlier or later w.r.t the linear ephemeris. The LTT effect can be measured with a high accuracy and used to infer the presence of planetary-mass companions around binary stars (Irwin 1952; Goździewski et al. 2012, 2015; Horner et al. 2012). In contrast to other techniques, the timing method is sensitive to massive extrasolar planets in long-period orbits. Futhermore, for low-mass binaries, the amplitude of the LTT effect increases (Ribas 2005; Pribulla et al. 2012).

Recently, a number of planetary-mass companions orbiting the cataclysmic variables (CVs) and post-common envelope binaries (PCEBs) have been reported. For instance, two planets for NN Ser (Beuermann et al. 2010) and UZ For (Potter et al. 2011), a single planet for DP Leo (Beuermann et al. 2011) and V470 Cam (Beuermann et al. 2012a) have been claimed. A long-term stable system of three planets hosted by HU Aqr, with the middle one being on a retrograde orbit, was recently proposed by Goździewski et al. (2015).

NSVS 14256825 was discovered through the Northern Sky Variability Survey (NSVS; Woźniak et al. 2004b). Wils et al. (2007) identified this system as an eclipsing binary with an amplitude of variations in the range of 13.22–14.03 (V). These authors also presented the first B, V, I_c light curves and physical parameters of this binary ($P = 0.110374230(2)$ days), along with a few eclipse times. NSVS 14256825 is a member of the HW Vir family (PCEB) consisting of an OB sub-dwarf and an M-dwarf companion (sdOB+dM; Almeida

et al. 2012). The following physical and geometrical parameters were obtained: $i = 82.^{\circ}5 \pm 0.^{\circ}3$ (inclination of the system), $M_1 = 0.419 \pm 0.070\ M_{\odot}$, $R_1 = 0.188 \pm 0.010\ R_{\odot}$, $M_2 = 0.109 \pm 0.023\ M_{\odot}$, $R_2 = 0.162 \pm 0.008\ R_{\odot}$ (the masses and radii of the components), and $a = 0.80 \pm 0.04\ R_{\odot}$ (separation between the components from the photometric and spectroscopic observations; Almeida et al. 2012).

The eclipse times of NSVS 14256825 have been reported by Wils et al. (2007), Kilkenny & Koen (2012), Beuermann et al. (2012a), Almeida et al. (2013), and Lohr et al. (2014). Qian et al. (2010) and Zhu et al. (2011) also argued for a O–C cyclic variation; however, they have not published any supporting data yet. Kilkenny & Koen (2012) reported an increasing orbital period of this system with a rate of $\sim 1.1 \times 10^{-10}$ ss^{-1}. Beuermann et al. (2012a) detected cyclic period changes and suggested the presence of a single CBP of $\sim 12\ M_{\rm Jup}$ with a period of $\sim$20 years. Almeida et al. (2013) presented a few additional eclipse times and argued for the presence of two CBPs with periods of $\sim$3.5 and $\sim$6.7 years, and masses of $\sim 3\ M_{\rm Jup}$ and $\sim 8.0\ M_{\rm Jup}$, respectively. Wittenmyer et al. (2013) presented a dynamical analysis of the orbital stability of the two-planet model proposed by Almeida et al. (2013). They found that this model is extremely unstable on a timescale of less than a thousand years. Moreover, Hinse et al. (2014) also performed a detailed data analysis of the timing measurements of this system. They concluded that the time span of eclipse time variations is not long enough to explain any particular one-planet model or to provide convincing evidence for a second planetary companion. Recently, Lohr et al. (2014) presented many new eclipse times of NSVS 14256825 from the SuperWASP archive. Their measurements obtained between 2006 and 2011 confirm the overall trend already seen in the O–C diagram.

In this study, we present 83 new mid-eclipse times of NSVS 14256825 obtained between 2009 August 21 and 2016 November 03 that together with the literature data give 153 eclipses over the time span of 17 years. We combined our new data with the previously published measurements to analyze the orbital period variations of this system. In Section 2, we present the observations and data reduction process together with the methodology used to obtain the eclipse times. Section 3 presents the procedure applied to examine the period variations, while the results are gathered in Section 4. In Sections 5 and 6, we discuss and conclude our findings. We include some additional materials in the Appendix. We also include four tables. Table 1 gives new eclipse times (Section 2), while Table 2 gives parameters of the third-body with linear ephemeris (Section 4). In the Appendix, we present observing log in Table 3 and a list of all NSVS 14256825 eclipse times from the literature together with our new measurements in Table 4.

2. New Photometry of NSVS 14256825

We performed photometric observations of NSVS 14256825 between 2009 August 21 and 2016 November 03 with five different telescopes: the 1.3 m telescope at the Skinakas Observatory (SKO, Creete, Greece), the 0.5 m telescope at the Astronomical Observatory of the Jagiellonian University (KRK, Kraków, Poland), the 0.6 m telescope at the Mt. Suhora Observatory (SUH, Koninki, Poland), the 0.6 m telescope at the Adiyaman University Observatory (ADYU60, Adiyaman, Turkey), and the 1 m telescope at the TUBITAK National Observatory (TUG, Antalya, Turkey).

Table 1
List of New NSVS 14256825 Eclipse Times

Cycle	BJD	Error (days)	Eclipse Type	Ref
7167.5	2455065.315208	0.000082	2	5
7204.0	2455069.343870	0.000036	1	5
7223.0	2455071.440996	0.000014	1	5
7386.0	2455089.432002	0.000024	1	6
7503.0	2455102.345843	0.000018	1	5
7557.0	2455108.306027	0.000041	1	5
7955.0	2455152.234856	0.000018	1	6

Note. In the columns, cycle number, time of the minimum and its corresponding error, as well as the type of the eclipse (1—primary, 2—secondary) and references are given. References correspond to the following observatories: (5) the Astronomical Observatory of the Jagiellonian University, (6) the Mt. Suhora Observatory, (7) the Skinakas Observatory, (8) the TUBITAK National Observatory, (9) the Adiyaman University Observatory.

(This table is available in its entirety in machine-readable form.)

Between 2009 and 2013, observations were performed using the SKO, KRK, and SUH telescopes, while those taken between 2014 and 2016, with the ADYU60 and TUG telescopes. We gathered data with the following CCD cameras: the Andor iKon DZ-936B-BV (KRK), the Andor DZ436 (SKO), the Apoge Alta U47 (SUH), the Andor iKon-M934 (ADYU60), and the SI1100 (TUG). A summary of observations is given in Table 3, where the start observing date, the cycle number, eclipse type (primary—1, secondary—2), filter used, exposure time, and readout time are listed.

The CCD data were reduced with the pipeline developed using Python, IRAF, and Sextractor software. The usual bias and dark subtraction as well as flat-field correction were applied to all images. For Andor CCDs, dark counts were negligible and therefore, only bias subtraction was done. A nearby constant star in the field of view, comparable to the target star in brightness and color, was chosen as the comparison star. Since our major goal was to obtain differential photometry only, we did not observe any photometric standard stars. For each night, a light curve was constructed consisting of extracted magnitude differences and time in the form of JD UTC. The mid-exposure times were taken.

We modeled the shapes of the eclipses with a modified and truncated inverted Gaussian $G(\tau)$ multiplied by a polynomial, as described in Section 2. of Beuermann et al. (2012a). The model involves eight parameters, including eclipse minimum time ($T_{\rm obs}$) denoted as p_1 in Beuermann et al. (2012a). The resulting parameter values and their respective uncertainties (including $\sigma_{T_{\rm obs}}$) were obtained from the fitting procedure as a term of the resulting covariance matrix from the nonlinear least squares fitting algorithm. Figure 8 shows the observed light curves and model fits. The derived eclipse times were converted to the barycentric dynamical time (BJD), using the FK5 sky coordinates of NSVS 14256825 ($\alpha = 20^{\rm h}20^{\rm m}00.^{\rm s}458$, $\delta = +04^{\circ}37'56.''50$) and the geodetic coordinates of each given observatory, with the help of the numerical procedure developed by Eastman et al. (2010). The eclipse minimum times, together with their respective errors, obtained from our new measurements are listed in Table 1, while all timings (including those published in the literature) are gathered in Table 4 (available in the on-line version only). The cycle numbers in Tables 1 and 4 are given according to the ephemeris from Beuermann et al. (2012a). We would like to note that we have three pairs of simultaneous observations of NSVS 14256825 with the TUG

and Adiyaman telescopes, i.e., these for cycle numbers: 30669, 30670, and 30931. For each pair, the difference between derived $T_{\rm obs}$ agrees within their errors derived from the fit, i.e., less than two seconds.

3. LTT Models of the (O–C)

To model the eclipses ephemeris with the presence of a hypothetical third body, we used the following formulae

$$T_{\rm eph}(L) = t_0 + P_{\rm bin}L + \gamma_{\rm tb}(L), \quad (1)$$

where $\gamma_{\rm tb}$ represents the LTT term (Irwin 1952). In our formulation, this term is parametrized by the Keplerian orbital elements of the third-body companion in orbit around the mass center of the binary (Goździewski et al. 2012):

$$\gamma_{\rm tb}(t) = K[\sin\omega(\cos E(t) - e) + \cos\omega\sqrt{1-e^2}\sin E(t)],$$

where K is the semi-amplitude of the LTT signal, e, ω, P, τ are the eccentricity, periastron argument, orbital period, and the time of periastron passage of the relative orbit of the putative companion w.r.t. the binary. We note that P and τ are introduced indirectly through the *Kepler* equation

$$\frac{2\pi}{P}(t-\tau) = E - e\sin E.$$

Due to very different timescales of orbital motion, the binary is represented as a point with the total mass of both stellar components equal to 0.528 $M_\odot$ (Almeida et al. 2012). Furthermore, to account for small eccentricity, we introduce Poincaré elements ($x \equiv e\cos\omega$, $y \equiv e\sin\omega$), which make it possible to get rid of weakly constrained eccentricity and pericenter argument ω for quasi-circular and moderately eccentric orbits.

To express the (O–C) variability through $\gamma_{\rm pl}(L(t))$, we optimize the likelihood function $\mathcal{L}$,

$$\log\mathcal{L}(\mathcal{D}|\boldsymbol{\xi}) = -\frac{1}{2}\chi^2 - \frac{1}{2}\sum_i N\log\sigma_i^2 - \frac{1}{2}N\log 2\pi, \quad (2)$$

where the χ^2 function

$$\chi^2(\mathcal{D},\boldsymbol{\xi}) = \sum_i^N \frac{[{\rm O}(\mathcal{D}) - {\rm C}(\boldsymbol{\xi})]_i^2}{\sigma_i^2} \quad (3)$$

depends on model parameters through $({\rm O-C})_i \equiv (T_{\rm obs}(L_i) - T_{\rm eph}(L_i))$ and the measurements uncertainties σ_i, where $i = 1 \ldots, N$ (Goździewski et al. 2015). Here, $({\rm O-C})_i$ denotes the deviation of the observed ith eclipse time-mark from its BJD ephemeris (Equation (1)) for cycle $L_i \equiv L(t_i)$. The model parameters vector $\boldsymbol{\xi} \equiv (K, P, e, \omega, \tau, P_{\rm bin}, t_0, \sigma_f)$, and N denotes the number of measurements encoded as data set $\mathcal{D}$. We note that all parameters of $T_{\rm eph}$ are optimized. This more general form of $\mathcal{L}$ also makes it possible to determine the free parameter σ_f that scales the raw uncertainties σ_i in quadrature, such that $\sigma_{i,t}^2 \to \sigma_i^2 + \sigma_f^2$ results in $\chi_\nu^2 \equiv \chi^2/(N - \dim\boldsymbol{\xi}) \sim 1$.

Optimization of the dynamical model relies on investigating the space of eight free model parameters $\boldsymbol{\xi}$, through sampling the posterior probability distribution $\mathcal{P}(\boldsymbol{\xi}|\mathcal{D})$ of the parameters $\boldsymbol{\xi}$, given the data set $\mathcal{D}$: $\mathcal{P}(\boldsymbol{\xi}|\mathcal{D}) \propto \mathcal{P}(\boldsymbol{\xi})\mathcal{P}(\mathcal{D}|\boldsymbol{\xi})$, where $\mathcal{P}(\boldsymbol{\xi})$ is the prior, and the sampling data distribution $\mathcal{P}(\mathcal{D}|\boldsymbol{\xi}) \equiv \log\mathcal{L}(\mathcal{D}|\boldsymbol{\xi})$. For all of these parameters, priors have been set as uniform (or uniform improper) through imposing parameter ranges available for exploration, i.e., K, P, $\tau > 0$ days, $\sigma_f > 0$ days,

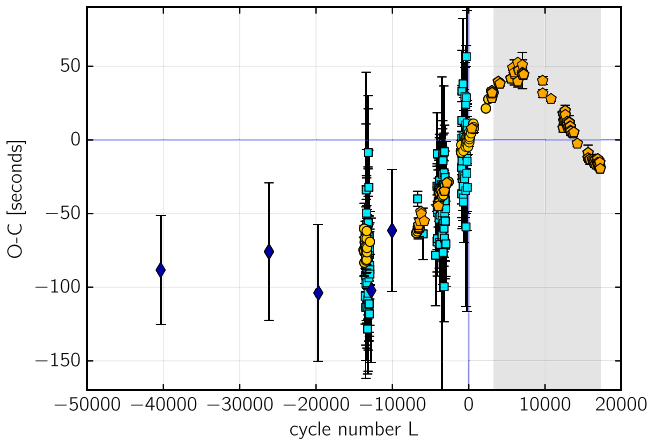

Figure 1. (O–C) diagram w.r.t. the linear ephemeris for Data Set A, with all data available in the literature. Filled rectangles are for raw (unbinned) SuperWASP data, filled circles and diamonds are for other measurements prior to epoch of 2012 August, and pentagons are for the new timing data in this paper (Table 1). See the text for details.

and $x, y \in [-0.71, 0.71]$, $P_{\rm bin} \in [0.110, 0.112]$ days, and $\Delta t_0 \in [-0.1, 0.1]$ days, which is for the displacement w.r.t. the cycle $L = 0$ for the epoch of $T_0 = {\rm BJD}\ 2455793.840061$.

We sampled the posterior with the Markov Chain Monte Carlo (MCMC) emcee package of the affine-invariant ensemble sampler (Goodman & Weare 2010), kindly provided by Foreman-Mackey et al. (2013).

4. LTT Model Results

Due to the non-homogeneous timing data, which are gathered across the literature and in this manuscript, we consider three data sets. Data Set A includes all observations available to date, which encompasses CCD observations and five measurements from the NSVS and ASAS archives in Beuermann et al. (2012a), SuperWASP-derived timing data (Lohr et al. 2014), as well as our new measurements listed in Table 1. Due to a large scatter and uncertainties, the SuperWASP measurements are finally excluded in Data Set B. In Data Set C, we also excluded the NSVS and ASAS measurements due to the uncertain derivation of these measurements, which is discussed in Section 5.1. Then, we subsequently analyzed Data Sets A, B, and C individually. These particular data sets are illustrated in the (O–C) diagrams in Figures 1, 2 and 3, respectively.

In all figures included in this section, we marked with gray rectangles the time interval after the last epoch in (Hinse et al. 2014), i.e., 2012 August, which indicates our new measurements. We may expect that the orbital period of a putative third object may be constrained and that changes the conclusions of Hinse et al. (2014), who were able to see only an increase of the (O–C).

Parameters of the linear ephemeris for Data Set A are

$$T_{\rm eph}(L) = {\rm BJD}\ 2455793.84004(2) + L\ 0.110374083(2),$$

for Data Set B, the linear ephemeris is described through

$$T_{\rm eph}(L) = {\rm BJD}\ 2455793.84005(3) + L\ 0.110374082(3),$$

while that for Data Set C is

$$T_{\rm eph}(L) = {\rm BJD}\ 2455793.84005(3) + L\ 0.110374082(3),$$

where $T_{\rm eph}$ stands here for the linear ephemeris of the BJD moment of the mid-eclipse of the cycle L. We chose the initial

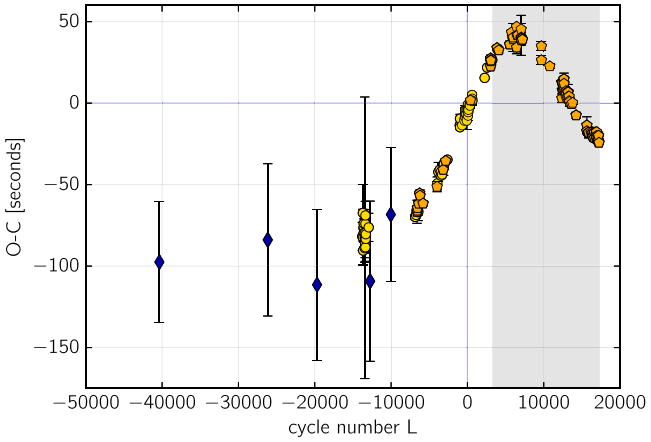

Figure 2. (O–C) diagram w.r.t. the linear ephemeris for Data Set B. Dark blue diamonds are for the NSVS and ASAS measurements, filled circles are for data in the up-to date literature excluding SuperWASP measurements, dark diamonds are for NSVS and ASAS data, and darker pentagons are for the new measurements in this paper (Table 1). See the text for details.

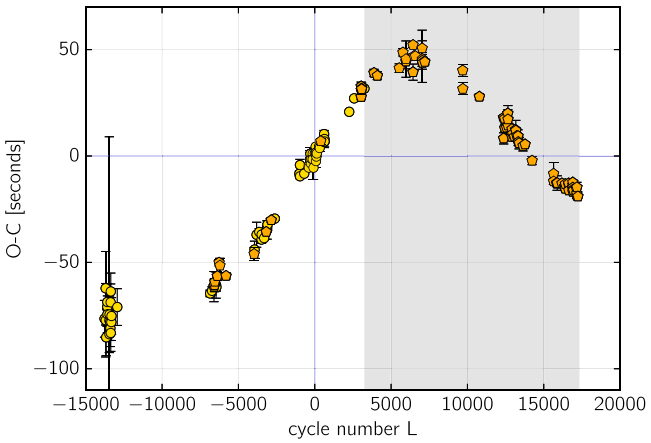

Figure 3. (O–C) diagram w.r.t. the linear ephemeris for Data Set C. Filled circles are for data in the up-to date literature excluding SuperWASP, NSVS and ASAS measurements, and pentagons are for the new timing data in this paper (Table 1). See the text for details.

epoch T_0 of the cycle $L = 0$ roughly in the middle of the observational window, i.e., $T_0 = \mathrm{BJD}\ 2455793.840061$. It is clear that the linear ephemeris is essentially the same, within the errors at the last significant digit marked in brackets. However, the SuperWASP, NSVS, and ASAS points strongly deviate from apparently a quasi-sinusoidal pattern formed by (O–C) derived from more accurate measurements.

Before sampling the posterior, which is determined through the likelihood function (Equation (2)), we first found the best-fitting parameters through maximizing $\mathcal{L}$ with the genetic algorithm (Charbonneau 1995). Next, we ran the MCMC sampler for 512 initial conditions inside a small ball centered on this solution. We tested chain lengths from 32,000 up to 768,000 samples. The latter, very large number of samples may be considered redundant, given the acceptance fraction of $\simeq$0.35, indicating an optimal output from the MCMC sampler (Foreman-Mackey et al. 2013).

The best-fitting models and their residuals are illustrated in the top and bottom panels of Figures 4, 5 and 6, for A, B, and C data sets, respectively. The posterior distribution is illustrated only for Data Set C (Figure 7), since the posteriors for Data Sets A and B are very similar, and therefore, to save space, we do not quote them. We note that the time of pericenter argument τ, the binary period $P_{\rm bin}$, and the time-shift Δt_0 from the cycle $L = 0$ epoch are represented relative to the best-fitting parameters in Table 2, respectively, where $T_0 = \mathrm{BJD}\ 2455793.840061$. These parameters are very close to the initial values derived with the common maximization of the likelihood function $\mathcal{L}$.

The posterior projections reveal relatively significant correlations of particular model parameters, like (K, P) and (P, τ). However, the posterior is uni-modal with a rather strong peak. This is illustrated in Figure 7 for a few selected parameters of the (O–C) model. The MCMC sampling reveals the error floor of $\simeq$2 s for models optimal in the sense defined above. Without this correction, the "raw" reduced $\chi^2_\nu \sim 2$ indicates underestimated uncertainties. The optimal solution is represented with a red curve, and is overplotted on 100 randomly selected model curves from the MCMC sample. We found that the eccentricity of the best-fitting orbit $e \simeq 0.175$, indicating a significantly skewed (O–C) curve, and a relatively large semi-amplitude of the LTT signal $K \simeq 50$ s, rule out pericenter precession of the orbit, following Beuermann et al. (2012a).

Due to apparently random residuals with an rms $\simeq$10 s, which is almost equal to the mean of the rescaled uncertainties, we did not analyze models with additional parameters, such as the parabolic ephemeris (Hinse et al. 2014) or even a putative second companion (Almeida et al. 2013). The most simple, 1-companion model with the linear ephemeris, does not exhibit systematic, long-term changes of the (O–C) superimposed on the quasi-sinusoidal variation. Secular changes of the orbital period should not be expected for such a detached binary (Beuermann et al. 2012a).

To infer the companion mass from the third-body model parameters listed in Table 2, we used the stellar masses as $M_1 = 0.419\,M_\odot$ and $M_2 = 0.109\,M_\odot$ for the primary and the secondary, respectively, following Almeida et al. (2012). The best-fitting orbital period of $P \simeq 3600$ days implies the minimal mass of $\sim$15 Jupiter masses (when the orbits are co-planar), that is in the brown dwarf. For the ratio of orbital periods $P/P_{\rm bin} \sim 4 \times 10^4$, the triple system is highly hierarchical. Obviously, the brown dwarf has a stable orbit, which is two orders of magnitude wider than the stability limit $\simeq$0.2 $a_{\rm bin}$ (roughly $\sim$0.01 au for the NSVS 14256825 binary) expected for circumbinary companions, if the binary eccentricity $e_{\rm bin} \simeq 0$ (e.g., Holman & Wiegert 1999, their Table 7). In such a case, the brown dwarf eccentricity $\sim$0.2 has a negligible impact on the stability.

The third-body parameters determined here substantially differ from previous estimates. For instance, Beuermann et al. (2012a) reported the orbital period unconstrained between 20 and 70 years with an eccentricity of $e \simeq 0.50$ for a 20 year orbit, since their data did not cover the (O–C) maximum revealed here. We determine the semi-amplitude of the LTT signal being roughly twice larger than that stated in Hinse et al. (2014). The amplitude of (O–C) is one of crucial parameters needed to estimate the energy required to support the Applegate cycles (e.g., Völschow et al. 2016).

5. Discussion

5.1. The NSVS and ASAS Timing Data

We would like to comment on the five earliest points from the literature, i.e., one timing measurement from the NSVS (Woźniak et al. 2004a) survey and four measurements from the

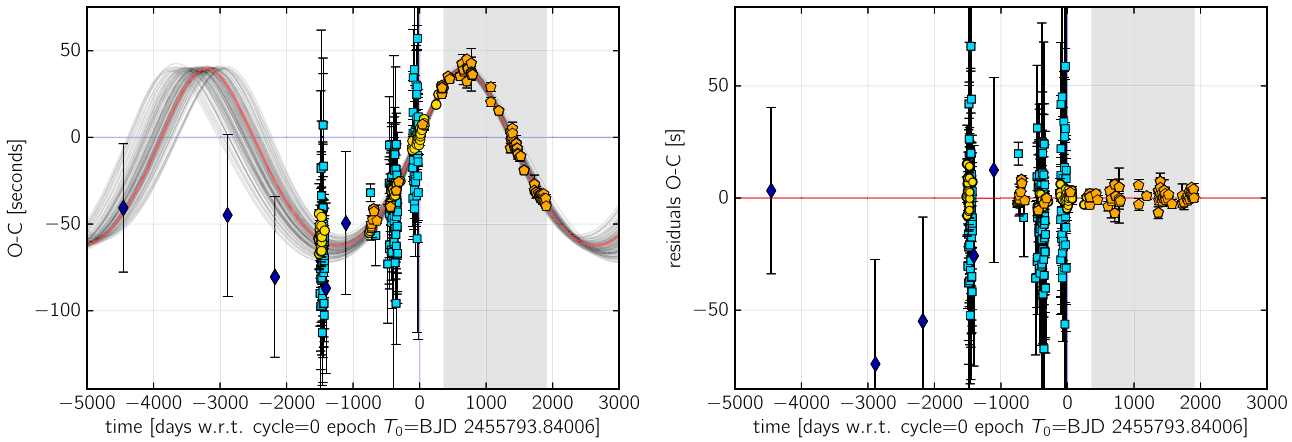

Figure 4. Top panel: the synthetic curve of the best-fitting model (red curve) to all timing data (Data Set A). Gray curves illustrate 100 randomly selected parameter samples from the MCMC posterior. Bottom panel: residuals to the best-fitting solution.

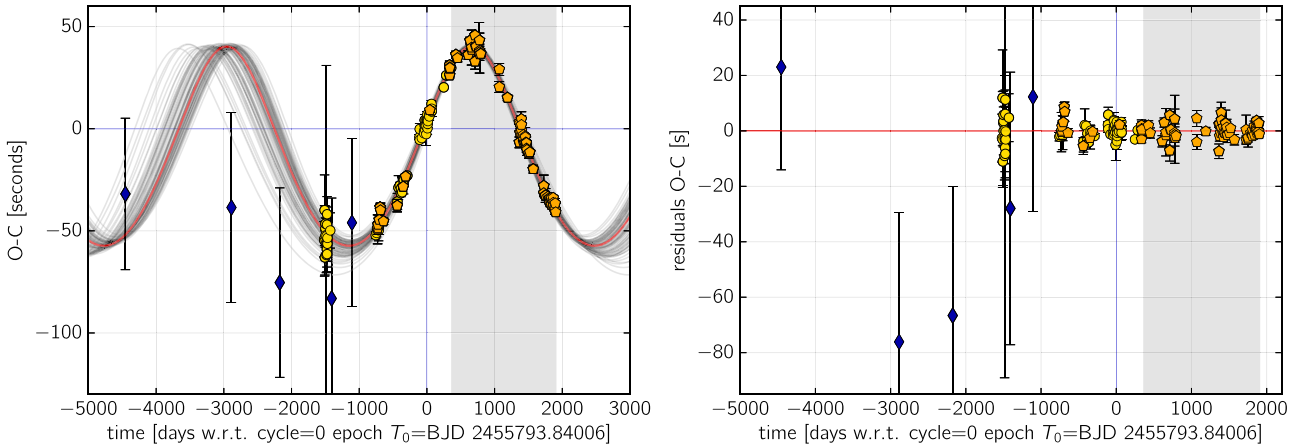

Figure 5. Top panel: the synthetic curve of the best-fitting model (red curve) to all data excluding SuperWASP data (Data Set B). Gray curves illustrate 100 randomly selected parameter samples from the MCMC posterior. Bottom panel: residuals to the best-fitting solution.

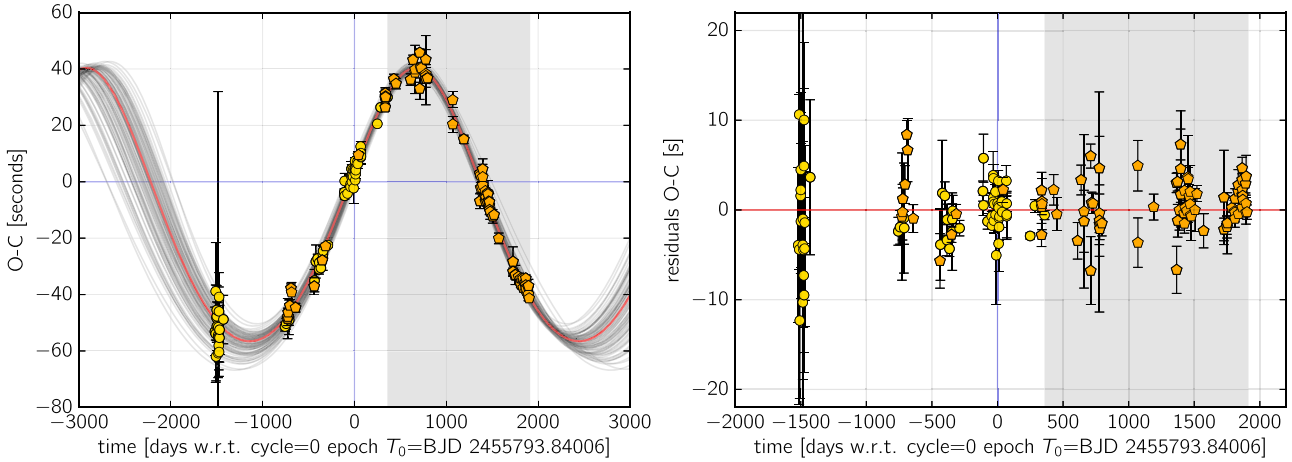

Figure 6. Top panel: the synthetic curve of the best-fitting model (red curve) to data without SuperWASP and NSVS/ASAS points (Data Set C). Gray curves illustrate 100 randomly selected parameter samples from the MCMC posterior. Bottom panel: residuals to the best-fitting solution displayed in Table 2.

ASAS survey (Pojmanski 1997), all five presented by Beuermann et al. (2012a).

It may be observed that these data exhibit large uncertainties and they strongly deviate from the models shown in this work. The exposure time is 80 s for the NSVS survey, and as long as 180 s for the ASAS light curves. Moreover, to derive eclipses, one must collect measurements by folding photometric points spanning over a whole year.

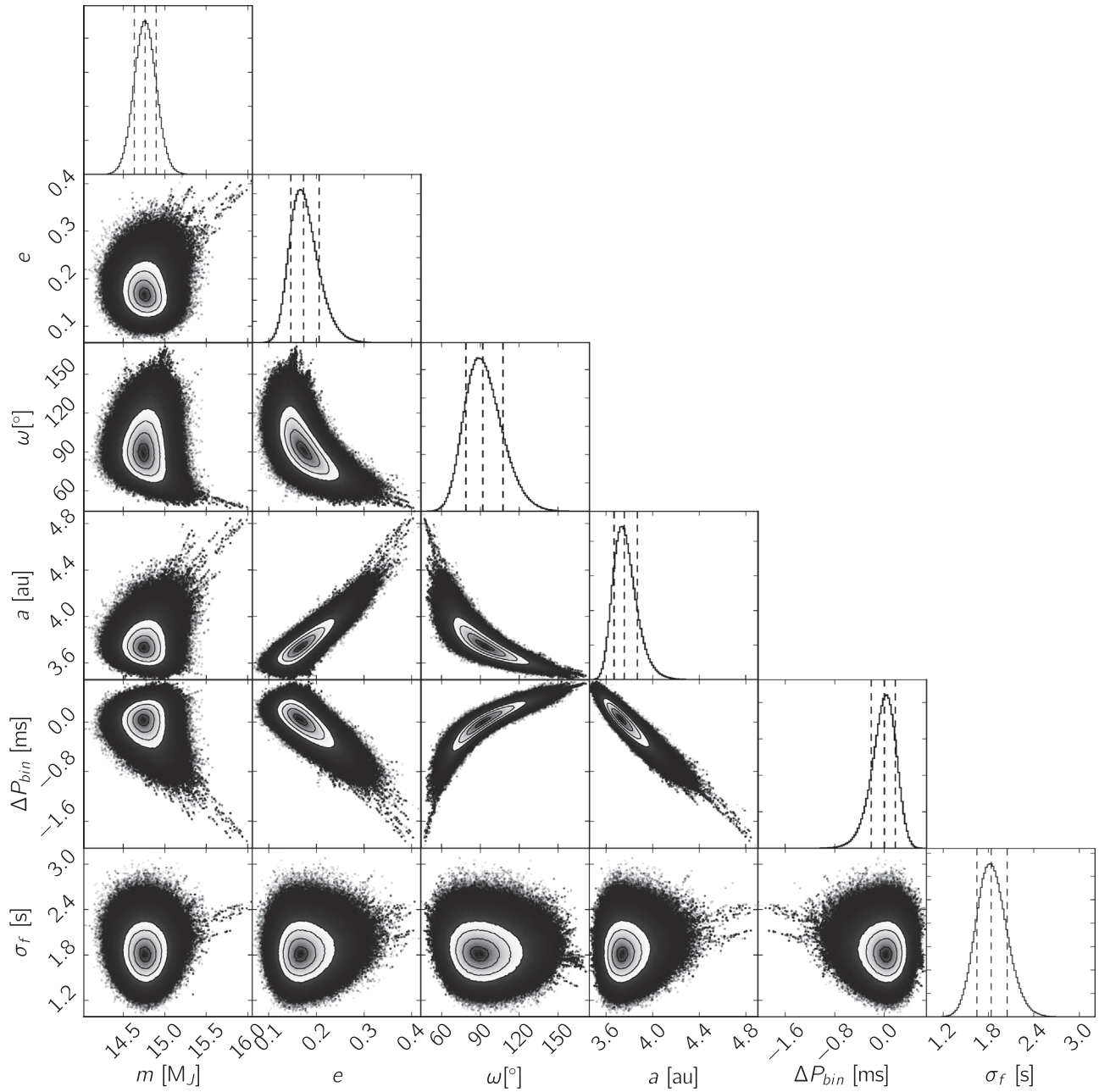

Figure 7. One- and two-dimensional projections of the posterior probability distributions of a few parameters inferred from the (O–C) model for Data Set C (Table 2 and Figure 6). There are illustrated 32,000 samples for 512 "walkers" initiated in a small ball around the best-fitting model in Table 2. We removed about of 10% initial, burn-out samples. Subsequent parameters are the companion mass m, eccentricity e, periastron argument ω, semimajor axis a, a deviation of the binary period $\Delta P_{\rm bin}$ from its adopted best-fitting value (in milliseconds, see Table 2), and the measurements uncertainty correction factor σ_f. Contours are for the 16th, 50th, and 84th percentile of samples in the posterior distribution. See the text for details regarding parametrisation of the (O–C) model and imposed priors. This figure was made using `corner.py` (Foreman-Mackey 2016).

Therefore, we decided to reanalyze the source photometric data to derive the timings in an independent way. We downloaded the source light curves from the publicly available NSVS[7] and ASAS[8] archives. The NSVS light curve spans epochs between 1999 and 2000, while the ASAS observations span over a few years between 2003 and 2008. The photometric NSVS measurements timestamps are given in MJD UTC, while the ASAS measurements in HJD UTC. Therefore, we recomputed the observation moments to the standard solar system barycenter BJD timescale with a procedure developed by Eastman et al. (2010). The data have been divided into $\sim$1 year intervals and phase-folded with the orbital period of the binary derived from the most recent linear ephemeris. We know that this period is determined with an uncertainty to a few milliseconds, and assuming that the linear ephemeris is valid, we may use this new, fixed estimate.

In the next step, we attempted to fit the function representing primary eclipses, as proposed in Beuermann et al. (2012a). We performed two experiments. In the first one, we fitted the whole set of parameters. In the second experiment, we constructed the

[7] http://skydot.lanl.gov/
[8] http://www.astrouw.edu.pl/asas/

Table 2
Parameters of the Third-body with Linear Ephemeris for Data Set C (Figures 6 and 7)

Parameter	Value	$+\sigma$	$-\sigma$
K (s)	48.9	1.6	1.2
P (day)	3632.8	169.6	131.7
x	0	0.045	0.042
y	0.175	0.032	0.031
τ (day)	7938.5	246.5	161.8
$P_{\rm bin}$ (day)	0.110374099	2×10^{-9}	3×10^{-9}
Δt_0 (day)	-5×10^{-5}	2×10^{-5}	2×10^{-5}
σ_f (s)	1.8	0.2	0.2
Mass ($M_{\rm Jup}$)	14.75	0.13	0.13
a (au)	3.74	0.12	0.09
e	0.175	0.012	0.003
ω (deg)	90.11	15.37	12.89

Note. Parameter Δt_0 is for the shift relative to the observational middle-window epoch T_0 = BJD 2455793.840061. Total mass of the binary is 0.528 $M_\odot$ (Almeida et al. 2012). See the text for details.

mean, synthetic light curve from the best 71 eclipses derived with the standard method. Then we fitted only some of the model eclipse parameters as free.

Unfortunately, all of these experiments resulted in variable mid-eclipses estimates spread over 90 s. Moreover, for the ASAS data, the O–C of our timing moments are systematically ∼60 second earlier than the measurements listed in Beuermann et al. (2012a).

The obtained formal errors from the model curve fits were on the level of ±35–42 s and are similar to the (O–C) deviations from the linear ephemeris. Also the folding of photometric data for a year (which is around 3300 binary cycles) introduces a systematic shift of the mid-eclipses, in accord with the local (O–C) trend. It could be as large as ∼20–50 s.

We conclude that the NSVS and ASAS mid-eclipse measurements are not very useful for the O–C analysis of such a short period binary. Fortunately, the parameters of our O–C models derived for each of the three data sets are similar. We believe that the final fit shown in Table 2, derived for Data Set C, does indeed represent a reliable solution.

5.2. The Applegate Mechanism of the (O–C)

For compact binaries, like NSVS 14256825, magnetic activity of the less massive component may trigger solar-like cycles and reshape the internal structure of this star (e.g., Applegate 1992; Lanza et al. 1998; Brinkworth et al. 2006). This leads to changes of the mutual gravitational field and oscillations of the orbital period. A common problem for this origin of the (O–C) variations is insufficient energy budget of the secondary required to change its quadrupole moment Q. Therefore, the Applegate cycles are usually dismissed in the literature as a possible explanation of cyclic variations of the (O–C) observed in a number of PCEBs. There are, however, more detailed and improved models of the Applegate mechanism, which modify the energy requirements (Lanza et al. 1998; Brinkworth et al. 2006; Lanza 2006). Recently, Völschow et al. (2016) considered a few variants of the Brinkworth et al. (2006) formulation that generally takes into account more realistic stellar density profiles. They analyzed a sample of 15 compact PCEBs, including NSVS 14256825, and found that only for four systems in the sample, the magnetic cycles may be responsible for the (O–C) behavior. For NSVS 14256825, the relative energy $\Delta E/E_{\rm sec}$ required to trigger the measured (O–C) should be between ∼5.4 for the "classic" Applegate model and ≃100 for an advanced model of the stellar density profile (for a constant density profile, the ratio is two orders of magnitude larger, ∼3000).

The up-to-date (O–C) analyzed in this paper implies a substantial change of the semi-amplitude K and the variation period, we recalculated estimates of the energy budget $\Delta E/E_{\rm sec}$ for NSVS 14256825 given in Völschow et al. (2016). We recomputed this value in accord with their Equation (7), following Tian et al. (2009), for canonical models in Applegate (1992) as well as for the modified Applegate mechanism in Lanza et al. (1998) and Lanza (2006, and references therein). We also used data for the secondary component from their Table 1.

Adopting the secondary radius $R_2 = 0.162\,R_\odot$, mass $M_2 = 0.109\,M_\odot$, orbital separation $a = 0.80\,R_\odot$, and the effective temperature $T = 2550$ K, we found that $\Delta E/E_{\rm sec} \simeq 11$. We computed the period change relative to the binary period

$$\frac{\Delta P}{P_{\rm bin}} = 4\pi\frac{K}{P} \simeq 2 \times 10^{-6},$$

with the semi-amplitude $K \simeq 49$ s and (O–C) oscillation $P \simeq 9.95$ years (modulation period) as displayed in Table 2. The quadrupole period variation ΔQ needed to drive the modulation of the orbital period (Lanza & Rodonò 1999) is

$$\frac{\Delta P}{P_{\rm bin}} = -9\frac{\Delta Q}{M_{\rm bin}a_{\rm bin}^2},$$

where $M_{\rm bin}$ and $a_{\rm bin}$ are the binary mass and the semimajor axis, respectively. For NSVS 14256825, we obtain the magnitude of $\Delta Q \simeq 10^{47}$ g cm^2.

The updated $\Delta E/E_{\rm sec}$ is more than two times larger than the value in Völschow et al. (2016) for the genuine Applegate model which, in accord with their analysis, tends to underestimate the energy ratio. For other variants, based on the Brinkworth et al. (2006) formulation, and realistic stellar density profiles, the Applegate modulations are even less probable, since the prescribed energy budget is then by one to two orders of magnitude too small, as shown in Völschow et al. (2016, their Table 4).

In accord with the alternative generalization of the Applegate mechanism by Lanza et al. (1998) and Lanza (2006), taking into account the additional factor of the Lorentz force, the magnetic cycles may operate with a fraction of the energy required by the original Applegate model. However, the lower limit of the calculated $\Delta E/E_{\rm sec} \sim 11$ factor even for this scenario seems to be so large that one can safely conclude that the Applegate mechanism and its generalizations proposed by Brinkworth et al. (2006), Lanza (2006), and Völschow et al. (2016) are not a credible explanations of the (O–C) variability in the NSVS 14256825 binary.

6. Conclusions

Our new set of light curves of the NSVS 14256825 binary substantially extends the archived list of eclipse timing. For the first time, our new data cover the maximum of the (O–C) w.r.t. the linear ephemeris, covering almost one full cycle of a quasi-sinusoidal modulation, and making it possible to put constrains

Table 3
NSVS 14256825 Observations Log: Starting Date of Observations, Cycle, Eclipse Type (1 for Primary, 2 for Secondary), Filter, Exposure Time, Readout Time and Observatory Code: KRK—the Astronomical Observatory of the Jagiellonian University, SUH—the Mt. Suhora Observatory, SKO—the Skinakas Observatory, TUG—the TUBITAK National Observatory, ADYU60—the Adiyaman University Observatory

Date	Cycle	Eclipse type	Filter	Exposure Time (s)	Readout (s)	Observatory
2009 Aug 21	7167.5	2	BG40	10	2.2	KRK
2009 Aug 25	7204.0	1	BG40	12	2.3	KRK
2009 Aug 27	7223.0	1	BG40	10	2.2	KRK
2009 Sep 14	7386.0	1	W-light	12	3.0	SUH
2009 Sep 27	7503.0	1	BG40	12	2.2	KRK
2009 Oct 03	7557.0	1	BG40	12	2.3	KRK
2009 Nov 16	7955.0	1	W-light	10	3.0	SUH

(This table is available in its entirety in machine-readable form.)

Table 4
List of the NSVS 14256825 Eclipse Times from the Literature as Well as New Measurements

	Cycle	BJD	Error (days)	Error (s)	Eclipse Type	Ref
1	−26586.0	2451339.803273	0.000429	37	1	2
2	−12390.0	2452906.673899	0.000541	47	1	2
3	−5931.0	2453619.579776	0.000537	46	1	2
4	0.0	2454274.208800	0.000100	9	1	1
5	72.0	2454282.155900	0.000200	17	1	1
6	73.0	2454282.266100	0.000200	17	1	1
7	108.0	2454286.129100	0.000100	9	1	1
8	172.0	2454293.193200	0.000100	9	1	1
9	180.0	2454294.076200	0.000100	9	1	1
10	181.0	2454294.186600	0.000100	9	1	1

Note. In the columns, the data point number, time of the minimum with its corresponding error, as well as the type of the eclipse (1 for primary, 2 for secondary) and references are given. References correspond to the following papers: (1) Wils et al. (2007), (2) Beuermann et al. (2012a), (3) Kilkenny & Koen (2012), (4) Almeida et al. (2013), (5) the astronomical observatory of the Jagiellonian University (this work), (6) the Mt. Suhora Observatory (this work), (7) the Skinakas Observatory (this work), (8) the TUBITAK National Observatory (this work), (9) the Adiyaman University Observatory (this work). Data from Lohr et al. (2014; see the Astro-ph version) are not included in this table.

(This table is available in its entirety in machine-readable form.)

on previousLTT models aimed at explaining the (O–C) behavior of this system (Beuermann et al. 2012a; Almeida et al. 2013; Hinse et al. 2014).

In accord with the third-body hypothesis, the observed (O–C) variations in the NSVS 14256825 may be explained by the presence of a single companion with a minimal mass in the brown dwarf mass range (14.7 Jupiter masses), in a moderately eccentric orbit with eccentricity $\simeq$0.2, and the orbital period of $\sim$10 years. We found that parameters of this third-body within our best model are relatively well constrained through the present data. The residuals do not indicate any significant secular trends, which could appear due to dissipative phenomena in the binary (like mass transfer, magnetic braking and gravitational radiation). We note that Beuermann et al. (2012a) and Hinse et al. (2014) reported such trends due to much shorter observational window that did not cover the maximum of the (O–C) shown in this work.

Therefore, a one-companion model may be the most reliable explanation of the NSVS 14256825 (O–C). Taking into account the updated amplitude of LTT of $K \simeq 50$ s and its period of $\simeq$10 years, the alternative hypothesis—the Applegate mechanism—does not seem to be sufficiently effective to produce such changes. In accord with a very recent analysis by Völschow et al. (2016), the energy required to trigger the Applegate cycles in the secondary companion should be 10–100 larger than its nuclear energy. Moreover, the relatively large K and the shape of (O–C) yielding the third-body orbit eccentricity of $\simeq$0.17, rule out also the orbital precession as a plausible (O–C) variation mechanism.

The presence of a massive companion in a moderately eccentric orbit around the evolved, compact binary would not necessarily be unusual on the grounds of the planet formation theory. Many scenarios are possible, regarding both first generation planets (companions) that survived the Common-Envelope (CE) phase, as well as emerged in a protoplanetary disk formed from the stellar matter ejected during the CE phase, as second generation of planets (e.g., Veras et al. 2011; Veras & Tout 2012; Portegies Zwart 2013; Bear & Soker 2014; Völschow et al. 2014; Kostov et al. 2016a; Veras et al. 2017). In the first case, the best-fitting orbital elements of NSVS 14256825 may be used as the border conditions required to reconstruct the binary evolution, as shown by Portegies Zwart (2013).

We do not analyze other possibilities of the (O–C) variability, like the mass transfer, orbital precession, magnetic braking, or gravitational radiation, which are usually refuted for this class of binaries.

We should stress, however, that the third-body hypothesis investigated for a number of close and evolved PCEBs reported in the literature, remains uncertain in most cases. A very

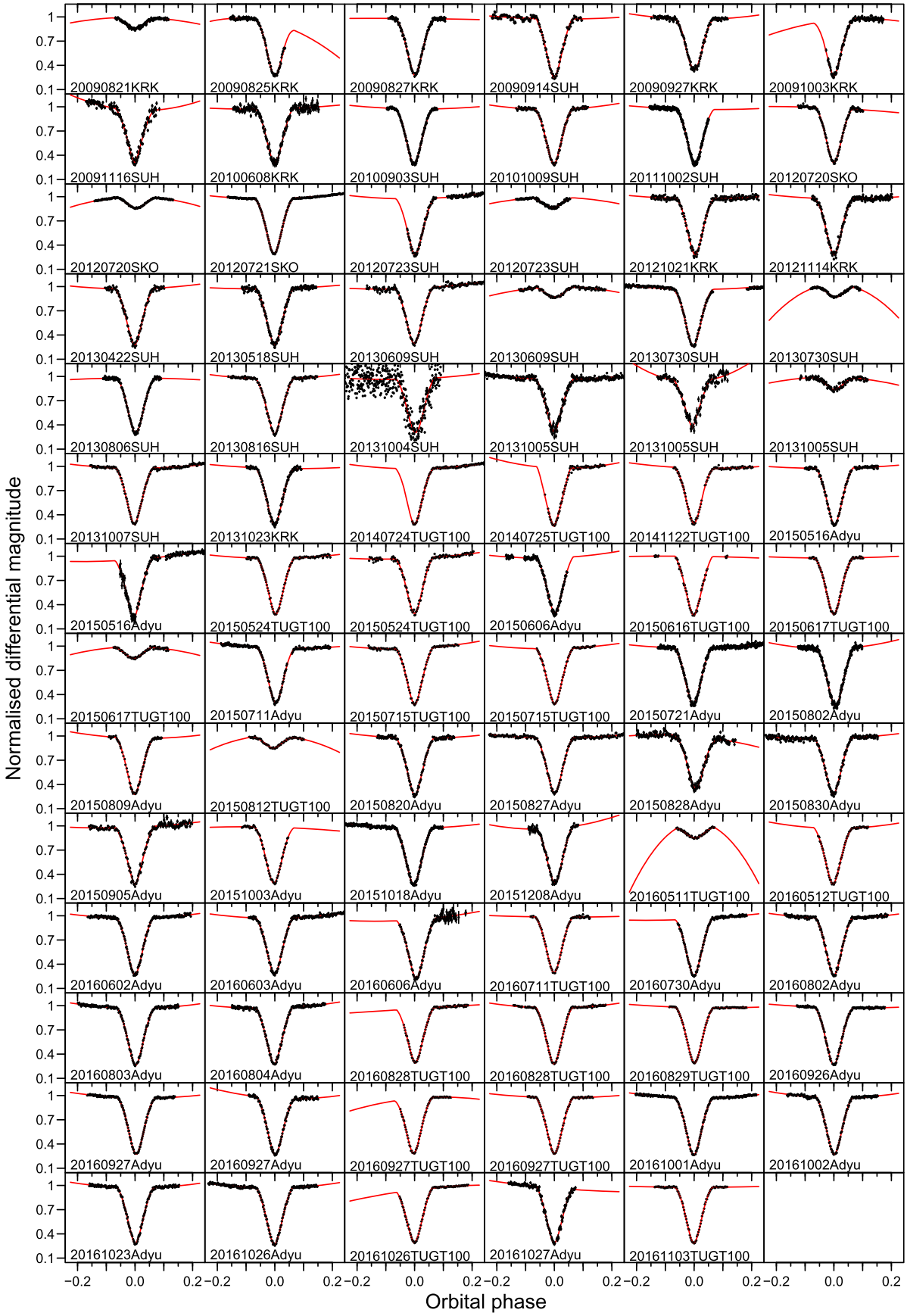

Figure 8. Primary and secondary eclipses of NSVS 14256825 from the 1 m telescope of the TUBITAK National Observatory (TUG), the 0.6 m telescope of the Adiyaman University Observatory (ADYU60), the 1.3 m telescope of the Skinakas Observatory (SKO), the 0.5 m telescope of the Astronomical Observatory of the Jagiellonian University (KRK), and the 0.6 m telescope of the Mt. Suhora Observatory (SUH), fitted with the equation as described in Section 2. of Beuermann et al. (2012a).

discouraging example of this kind is the CV polar, HU Aqr (Schwope et al. 1993; Schwarz et al. 2009; Qian et al. 2011; Goździewski et al. 2012; Hinse et al. 2012; Bours et al. 2014; Schwope & Thinius 2014; Goździewski et al. 2015). The apparently quasi-sinusiodal (O–C) variations with a full amplitude of ∼60 s observed for almost 20 years until 2012, has changed to a strong, secular trend that deviates by 180 s from the linear ephemeris to date. Two and three planet models of this system are strongly unstable, unless we consider an exotic system of three 5–6 $M_{\rm Jup}$ mass planets, with the middle one revolving in a retrograde orbit. Such a system may be stable for at least 1 Gyr (Goździewski et al. 2015). Similarly, the (O–C) of HW Vir interpreted through 5:2 MMR configuration of two Jovian planets (Beuermann et al. 2012b) are not constrained, regarding the outermost planet and its mass. The (O–C) for other PCEBs, like NY Vir (Qian et al. 2012b; Lee et al. 2014), QS Vir (Horner et al. 2013), and UZ For (Potter et al. 2011), could be formally explained with the resonant two-planet systems, yet none of them has been found stable. An exception is the NN Ser with low-mass, Jovian planets close to 2:1 mean motion resonance, which is well documented and has passed all tests of the planetary nature of the (O–C) so far (Beuermann et al. 2010; Marsh et al. 2014; Völschow et al. 2014). A few other PCEBs, like V471 Tau (Hardy et al. 2015), V470 Cam (Qian et al. 2013), RR Cae (Qian et al. 2012a) might host single-companions, see Almeida et al. (2013) and Zorotovic & Schreiber (2013) listing such binaries with their astrophysical characteristics.

Observations of these systems is still timely since the long-term, hardly predictable (O–C) are typically known for a fraction of the longest putative orbital periods. There are open problems regarding the PCBEs, like the formation of putative companions as first- or second-generation planets, orbital architectures, and stability of hypothetical multiple-companion configurations, the presence of mechanisms alternative or coexisting with the Applegate and Lanza–Rodonó cycles and the LTT effect. Therefore, while the planetary hypothesis of the (O–C) observed for NSVS 14256825 cannot be definite yet, our observations and new data may contribute more light on the unresolved astrophysical questions. For instance, the (O–C) amplitude constrains the energy required to trigger magnetic cycles of the M-dwarf component.

Additional, long-term timing observations of the NSVS 14256825 binary are required. Being relatively bright, the NSVS 14256825 system may be systematically monitored, as we show here, with ∼1 m class telescopes. During the next two to three years, the third-body model and the eclipse ephemeris can be verified due to (O–C) approaching the nearby minimum (see Figure 3 for our prediction).

We thank to the anonymous reviewer for critical and informative comments, which improved this work. This work has been supported by The Scientific and Technological Research Council of Turkey (TUBITAK), through project number 114F460 (I.N., A.S., H.E.). This work has been supported by Polish National Science Centre grant DEC-2011/03/D/ST9/00656 (A.S., K.K., M.Ż.) and MAESTRO grant DEC-2012/06/A/ST9/00276 (K.G.). We thank the team of TUBITAK National Observatory (TUG) for a partial support in using T100 telescope with project number TUG T100-631. We also wish to thank Adiyaman University Observatory (Turkey) and the Skinakas Observatory (Heraklion, Greece) teams. K.G. thanks the staff of the Poznan Supercomputer and Network Centre (PCSS) for the support and computational resources (grant 195).

Facility: Skinakas:1.3m.

Software: Python, IRAF, SExtractor, emcee (Foreman-Mackey et al. 2013), corner.py (Foreman-Mackey 2016).

Appendix
Additional Figures and Tables

The data for the 83 light curves presented in Figure 8 are provided as CSV files in a supplementary tar.gz archive. Each light curve consists of four columns (column names are given in brakets): JD UTC (time), differential magnitude value (dmag), differential magnitude error (ddmag), and phase calculated according to the linear ephemeris given by Equation (12) of Hinse et al. (2014; phase). Reuse of these light curves for publication requires permission from TUBITAK. In that case, please contact Ilham Nasiroglu inasir@atauni.edu.tr.

References

Almeida, L. A., Jablonski, F., & Rodrigues, C. V. 2013, ApJ, 766, 11
Almeida, L. A., Jablonski, F., Tello, J., & Rodrigues, C. V. 2012, MNRAS, 423, 478
Applegate, J. H. 1992, ApJ, 385, 621
Bear, E., & Soker, N. 2014, MNRAS, 444, 1698
Beuermann, K., Breitenstein, P., Debski, B., et al. 2012a, A&A, 540, A8
Beuermann, K., Buhlmann, J., Diese, J., et al. 2011, A&A, 526, A53
Beuermann, K., Dreizler, S., Hessman, F. V., & Deller, J. 2012b, A&A, 543, A138
Beuermann, K., Hessman, F. V., Dreizler, S., et al. 2010, A&A, 521, L60
Bours, M. C. P., Marsh, T. R., Breedt, E., et al. 2014, MNRAS, 445, 1924
Brinkworth, C. S., Marsh, T. R., Dhillon, V. S., & Knigge, C. 2006, MNRAS, 365, 287
Charbonneau, P. 1995, ApJS, 101, 309
Deeg, H. J., Ocaña, B., Kozhevnikov, V. P., et al. 2008, A&A, 480, 563
Doyle, L. R., Carter, J. A., Fabrycky, D. C., et al. 2011, Sci, 333, 1602
Eastman, J., Siverd, R., & Gaudi, B. S. 2010, PASP, 122, 935
Foreman-Mackey, D., Hogg, D. W., Lang, D., & Goodman, J. 2013, PASP, 125, 306
Foreman-Mackey, D. 2016, corner.py: Scatterplot matrices in Python, https://doi.org/10.21105/joss.00024
Goodman, J., & Weare, J. 2010, Comm. Apl. Math and Comp. Sci., 1, 65
Goździewski, K., Nasiroglu, I., Słowikowska, A., et al. 2012, MNRAS, 425, 930
Goździewski, K., Słowikowska, A., Dimitrov, D., et al. 2015, MNRAS, 448, 1118
Hardy, A., Schreiber, M. R., Parsons, S. G., et al. 2015, ApJL, 800, L24
Hinse, T. C., Lee, J. W., Goździewski, K., et al. 2012, MNRAS, 420, 3609
Hinse, T. C., Lee, J. W., Goździewski, K., Horner, J., & Wittenmyer, R. A. 2014, MNRAS, 438, 307
Holman, M. J., & Wiegert, P. A. 1999, AJ, 117, 621
Horner, J., Hinse, T. C., Wittenmyer, R. A., Marshall, J. P., & Tinney, C. G. 2012, MNRAS, 427, 2812
Horner, J., Wittenmyer, R. A., Hinse, T. C., et al. 2013, MNRAS, 435, 2033
Irwin, J. B. 1952, ApJ, 116, 211
Kilkenny, D., & Koen, C. 2012, MNRAS, 421, 3238
Kostov, V. B., Moore, K., Tamayo, D., Jayawardhana, R., & Rinehart, S. A. 2016a, ApJ, 832, 183
Kostov, V. B., Orosz, J. A., Welsh, W. F., et al. 2016b, ApJ, 827, 86
Lanza, A. F. 2006, MNRAS, 369, 1773
Lanza, A. F., & Rodonò, M. 1999, A&A, 349, 887
Lanza, A. F., Rodono, M., & Rosner, R. 1998, MNRAS, 296, 893
Lee, J. W., Hinse, T. C., Youn, J.-H., & Han, W. 2014, MNRAS, 445, 2331
Lee, J. W., Kim, S.-L., Kim, C.-H., et al. 2009, AJ, 137, 3181
Lohr, M. E., Norton, A. J., Anderson, D. R., et al. 2014, A&A, 566, A128
Marsh, T. R., Parsons, S. G., Bours, M. C. P., et al. 2014, MNRAS, 437, 475
Pojmanski, G. 1997, AcA, 47, 467
Portegies Zwart, S. 2013, MNRAS, 429, L45

Potter, S. B., Romero-Colmenero, E., Ramsay, G., et al. 2011, MNRAS, 416, 2202
Pribulla, T., Vaňko, M., Ammler-von Eiff, M., et al. 2012, AN, 333, 754
Qian, S.-B., Liu, L., Liao, W.-P., et al. 2011, MNRAS, 414, L16
Qian, S.-B., Liu, L., Zhu, L.-Y., et al. 2012a, MNRAS, 422, 24
Qian, S.-B., Shi, G., Zola, S., et al. 2013, MNRAS, 436, 1408
Qian, S.-B., Zhu, L.-Y., Dai, Z.-B., et al. 2012b, ApJL, 745, L23
Qian, S.-B., Zhu, L.-Y., Liu, L., et al. 2010, Ap&SS, 329, 113
Ribas, I. 2005, in ASP Conf. Ser. 335, The Light-Time Effect in Astrophysics: Causes and Cures of the O–C Diagram, ed. C. Sterken (San Francisco, CA: ASP), 55
Schwarz, R., Schwope, A. D., Vogel, J., et al. 2009, A&A, 496, 833
Schwope, A. D., & Thinius, B. D. 2014, AN, 335, 357
Schwope, A. D., Thomas, H. C., & Beuermann, K. 1993, A&A, 271, L25
Tian, Y. P., Xiang, F. Y., & Tao, X. 2009, Ap&SS, 319, 119
Veras, D., Georgakarakos, N., Dobbs-Dixon, I., & Gänsicke, B. T. 2017, MNRAS, 465, 2053
Veras, D., & Tout, C. A. 2012, MNRAS, 422, 1648
Veras, D., Wyatt, M. C., Mustill, A. J., Bonsor, A., & Eldridge, J. J. 2011, MNRAS, 417, 2104
Völschow, M., Banerjee, R., & Hessman, F. V. 2014, A&A, 562, A19
Völschow, M., Schleicher, D. R. G., Perdelwitz, V., & Banerjee, R. 2016, A&A, 587, A34
Wils, P., di Scala, G., & Otero, S. A. 2007, IBVS, 5800, 1
Wittenmyer, R. A., Horner, J., & Marshall, J. P. 2013, MNRAS, 431, 2150
Woźniak, P. R., Vestrand, W. T., Akerlof, C. W., et al. 2004a, AJ, 127, 2436
Woźniak, P. R., Williams, S. J., Vestrand, W. T., & Gupta, V. 2004b, AJ, 128, 2965
Zhu, L., Qian, S., Liu, L., et al. 2011, in ASP Conf. Ser. 451, 9th Pacific Rim Conference on Stellar Astrophysics, ed. S. Qain et al. (San Francisco, CA: ASP), 155
Zorotovic, M., & Schreiber, M. R. 2013, A&A, 549, A95